AD-A031 974 NAVAL ELECTRONICS LAB CENTER SAN DIEGO CALIF F/G 17/1
EVALUATION OF A XONICS ACOUSTIC ECHOSOUNDER AND WIND-SENSOR SYS--ETC(U)
JUL 76 D R JENSEN, J H RICHTER
UNCLASSIFIED NELC/TR-1997 NL

1 OF 1
AD A031974

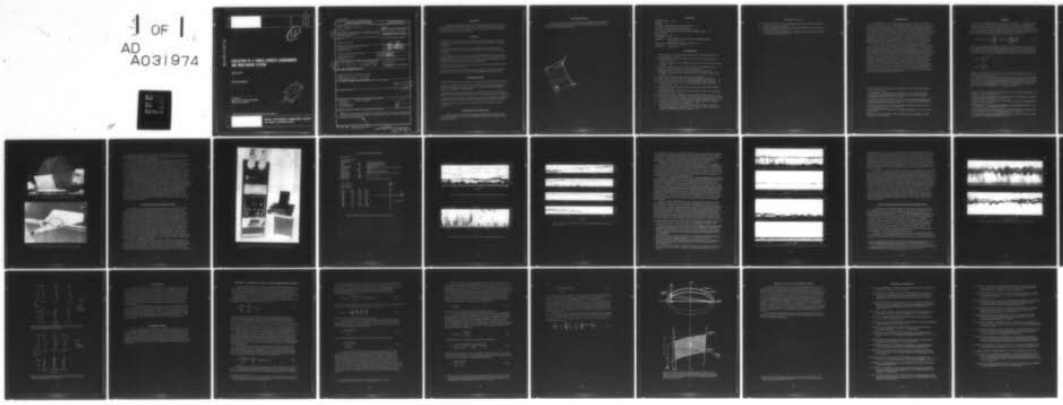

END
DATE FILMED
1 -77

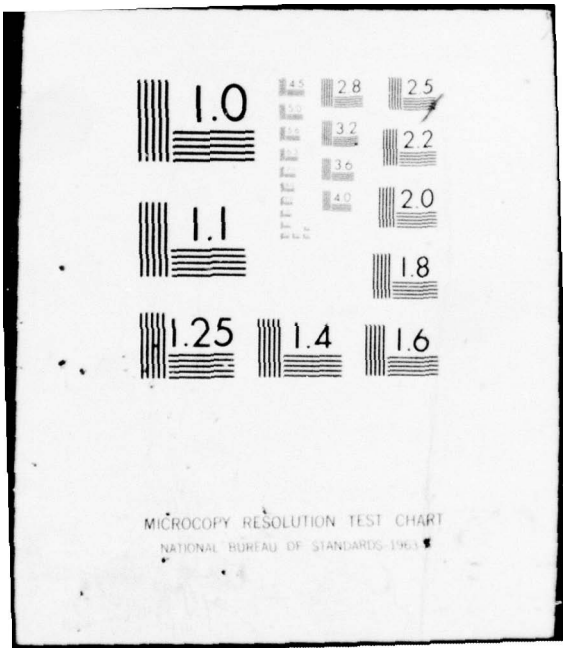
1.0
1.1
1.25
1.4
1.6
1.8
2.0
2.2
2.5
2.8
3.2
3.6
4.0
4.5
MICROCOPY RESOLUTION TEST CHART
NATIONAL BUREAU OF STANDARDS 1963

NELC / TR 1997

12

EVALUATION OF A XONICS ACOUSTIC ECHOSOUNDER AND WIND-SENSOR SYSTEM

26 July 1976

Test and Evaluation

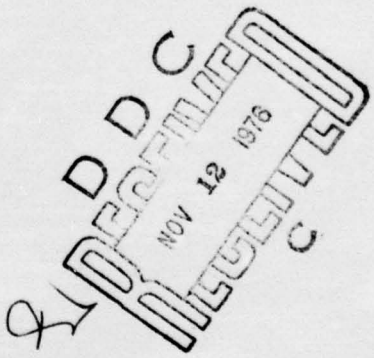

Prepared for
NAVAL AIR SYSTEMS COMMAND
Washington, DC 20361

APPROVED FOR PUBLIC RELEASE; DISTRIBUTION IS UNLIMITED.

NAVAL ELECTRONICS LABORATORY CENTER
SAN DIEGO, CALIFORNIA 92152

UNCLASSIFIED

SECURITY CLASSIFICATION OF THIS PAGE (When Data Entered)

REPORT DOCUMENTATION PAGE

READ INSTRUCTIONS BEFORE COMPLETING FORM

1. REPORT NUMBER: NELC Technical Report 1997 (TR 1997)

2. GOVT ACCESSION NO.

3. RECIPIENT'S CATALOG NUMBER

4. TITLE (and Subtitle): EVALUATION OF A XONICS ACOUSTIC ECHOSOUNDER AND WIND-SENSOR SYSTEM

5. TYPE OF REPORT & PERIOD COVERED: Test and Evaluation rept.

6. PERFORMING ORG. REPORT NUMBER

7. AUTHOR(s): DR Jensen and JH Richter

8. CONTRACT OR GRANT NUMBER(s)

9. PERFORMING ORGANIZATION NAME AND ADDRESS: Naval Electronics Laboratory Center, San Diego, CA 92152

10. PROGRAM ELEMENT, PROJECT, TASK AREA & WORK UNIT NUMBERS: 61153N WR03302 WR0330201 (NELC M111)

11. CONTROLLING OFFICE NAME AND ADDRESS: Naval Air Systems Command, Washington, DC 20361

12. REPORT DATE: 26 July 1976

13. NUMBER OF PAGES: 34

14. MONITORING AGENCY NAME & ADDRESS (if different from Controlling Office)

15. SECURITY CLASS. (of this report): UNCLASSIFIED

15a. DECLASSIFICATION/DOWNGRADING SCHEDULE

16. DISTRIBUTION STATEMENT (of this Report)

Approved for public release; distribution is unlimited.

NELC/TR-1997

17. DISTRIBUTION STATEMENT (of the abstract entered in Block 20, if different from Report)

18. SUPPLEMENTARY NOTES

19. KEY WORDS (Continue on reverse side if necessary and identify by block number)

Radar Echoes
Acoustic echoes
Electromagnetic sensors
Electro-optical sensors
Troposphere propagation

20. ABSTRACT (Continue on reverse side if necessary and identify by block number)

XONICS acoustic echosounder and wind-sensor system has the capability of simultaneously measuring temperature fluctuations in the lower atmosphere and the three wind components as a function of altitude. Reliable wind measurements are rarely obtainable.

DD FORM 1 JAN 73 1473 EDITION OF 1 NOV 65 IS OBSOLETE S/N 0102-LF-014-6601

UNCLASSIFIED

SECURITY CLASSIFICATION OF THIS PAGE (When Data Entered)

403 940

OBJECTIVE

Test and evaluate a XONICS Inc acoustic echosounder and wind-sensor system purchased by NELC (Contract Number N00123-73-C-2037). The system is designed to measure in real time the three orthogonal components of the total wind vector and the intensity of backscattered echoes as a function of elevation.

RESULTS

1. Monostatic acoustic echosounder records show atmospheric microstructure including internal waves, multiple stratified layering, cloud-top echoes, Kelvin-Helmholtz instabilities, and turbulence.

2. The acoustic echosounder is an important complement for the interpretations of the refractive structures observed by microwave radars and gives an indication of dynamic thermal stability.

3. The XONICS acoustic wind-sensing system has the fundamental capability of measuring all three components of the total wind vector. However, reliable wind-sensor measurements with the presently configured system have been obtained only for selected conditions characterized by low ambient background noise (see Appendix B).

4. The fan-beam bistatic receiving antennas appear to constitute the principal limiting factor in the acoustic wind-sensor system.

5. The above-ground bistatic receiving antenna further limits the operation of the system because of its reception of wind noise and ambient background returns from sidelobes.

RECOMMENDATIONS

1. Redesign the bistatic receiving antennas to incorporate pencil beams rather than fan beams.

2. Relocate the above-ground, bistatic, receiving antennas to bunkers with openings flush with the surrounding terrain to reduce the effects of wind noise and ambient background returns from the sidelobes (see Appendix B).

3. Incorporate frequency-tracking and cross-correlation techniques into software data processing to eliminate doppler spectrum contamination caused by impulsive noise (see Appendix B).

4. Initiate a study to determine the full potential of acoustic echosounding for the interpretation and prediction of atmospheric parameters affecting the Navy's operating environment.

5. Compare the capabilities of acoustic sounders with those of FM-CW radars for Navy operational use.

ADMINISTRATIVE INFORMATION

Work was performed for the Naval Air Systems Command under Program Element 61153N, Project WR03302, and Task Area WR0330201 (NELC M111) by members of the Propagation Division.

ACKNOWLEDGMENTS

The authors appreciate discussions with RJ Keeler and DE Hunter, WPL, NOAA Environmental Research Laboratories, and the assistance of WK Horner and ML Phares in the testing and evaluation of the sounder.

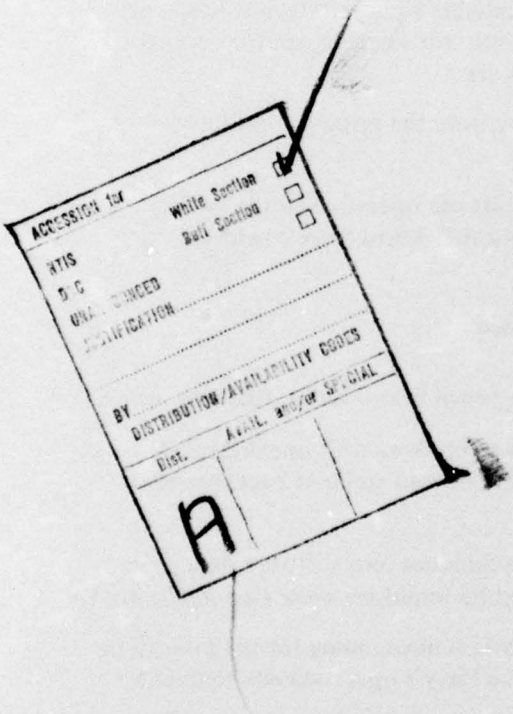

CONTENTS

ILLUSTRATIONS

Illustrations (Continued)

INTRODUCTION

Naval operations are critically dependent upon reliable performance of all electromagnetic and electro-optical sensors. For example, problems are continually encountered as a result of refractive effects upon electromagnetic propagation. Nonstandard refractive-index distributions in the lower atmosphere can and do cause anomalous propagation conditions such as ducting and radar holes. Similarly, temperature fluctuations and aerosols may degrade the performance of electro-optical sensors. During recent years, investigators have demonstrated the feasibility of using radio, optical, and acoustical techniques for remotely sensing atmospheric structures in the lower atmosphere (ref 1 through 6). The Naval Electronics Laboratory Center (NELC), at San Diego, California, has developed a unique multisensor facility capable of measuring the marine boundary-layer structures to improve the Navy's assessment and prediction capability for anomalous propagation in the troposphere.

In 1973, an acoustic echosounder and wind-sensor system (purchased from XONICS Inc, Van Nuys, CA) was added to the NELC remote-sensing facility to be used in conjunction with the tropospheric, microwave-radar sounder. The acoustic sounder senses temperature and if operated in a bistatic configuration, also tracks the wind-related, refractive-index fluctuations. The microwave-radar sounder primarily senses humidity fluctuations. The acoustic sounder, therefore, complements the microwave sounder and provides important additional information concerning the behavior and nature of the atmospheric structure. Acoustic sounding is a rapidly growing remote-sensing technique, and a full examination of its potential for the interpretation and prediction of atmospheric parameters affecting the Navy's operating environment should be accomplished. It is the purpose of this report to present the results of the test and evaluation, conducted over a 2-year period, of the XONICS echosounder and wind-sensor system. The sounder was designed to measure simultaneously, in near real time, the three orthogonal components of the total wind vector up to 600 metres and the backscatter from temperature fluctuations.

1. Lane, JA and RW Meadows, "Simultaneous Radar and Refractometer Soundings of the Troposphere," Nature, v 197, p 35-36, 1963
2. Atlas, D, KR Hardy, and KM Glover, "Multi-wavelength Backscatter from the Clear Atmosphere," Proceedings of the International Colloquium on Atmospheric Turbulence and Radio Propagation (Eds Yaglom and Tatavaski, Moscow)," p 249-260, 1965
3. Ottersten, H and F Eklund, "Radar Angle Activity and Its Correlation with Meteorological Parameters," Proceedings of the International Colloquium on Atmospheric Turbulence and Radio Propagation (Eds Yaglom and Tatavaski, Moscow)," p 269-277, 1965
4. Fehlhaber, L and S Grosskopf, "Untersuchung der Struktur der Troposphäre mit einem Vertikalradar," Nachrichtentechnische Zeitschrift, v 17, p 503-507, 1964
5. Richter, JH, "High Resolution Tropospheric Radar Sounding," Radio Science, v 4, no 12, p 1261-1268, December 1969
6. McAllister, LG, "Acoustic Sounding at the Lower Troposphere," Journal of Atmospheric Terrestrial Physics, v 30, p 1439-1440, 1968

THEORY

An extensive bibliography on the scattering of sound in the free atmosphere is given by Little (ref 7). The primary scattering mechanism for sound within the atmosphere is caused by refractive-index fluctuations from turbulent eddies. Temperature or wind fluctuations change the acoustic refractive index of the atmosphere and acoustic energy is scattered when such inhomogeneities are encountered. The theory of scattering for sound leads to an analytical equation governing the scattering cross section (ref 8 through 12):

$$\sigma(\theta) = 0.055\,\lambda^{-1/3}\cos^2\theta\left[\frac{C_V^2}{C^2}\cos^2\frac{\theta}{2} + 0.13\,\frac{C_T^2}{T^2}\right]\left(\sin\frac{\theta}{2}\right)^{-11/3}, \qquad (1)$$

where $\sigma(\theta)$ is the scattered power per unit volume per unit incident flux per unit solid angle at a scattering angle θ; λ is the acoustic wavelength; C is the mean velocity of sound in the scattering region; T is the mean temperature of the scattering region; and C_V and C_T are the structure constants for velocity and temperature, respectively. C_V and C_T are defined by:

$$C_V^2 = \frac{\overline{(U_1 - U_2)^2}}{r^{2/3}}$$

$$C_T^2 = \frac{\overline{(T_1 - T_2)^2}}{r^{2/3}},$$

where $\overline{(U_1 - U_2)}$ and $\overline{(T_1 - T_2)}$ are the rms velocity and temperature differences between two points separated by a distance r.

Equation (1) shows that the scattered acoustic power is a function of the wavelength ($\lambda^{-1/3}$), is dependent upon the sum of wind fluctuations (normalized by the mean velocity of sound in the medium) and temperature fluctuations (normalized by the mean temperature of the medium), and is dependent upon the direction in which scattering occurs (θ). For the monostatic or backscatter mode ($\theta = \pi$), equation (1) reduces to:

---

7. Little, CG, "Acoustic Methods for the Remote Probing of the Lower Atmosphere," Proceedings of the IEEE, v 57, no 6, p 571-578, April 1969

8. Lighthill, MJ, "On the Energy Scattered from the Interaction of Turbulence with Sound or Shock Waves," Proceedings of the Philosophical Society, v 49, p 531-555, 1953

9. Kraichnan, RH, "The Scattering of Sound in a Turbulent Medium," Journal of the Acoustical Society of America, v 25, p 1096-1104, 1953

10. NAS-NRC Publication 515, Proceedings of the Symposium on Naval Hydrodynamics, "Wave Scattering Due to Turbulence," by GK Bachelor, p 409-430, 1957

11. Monin, AS, "Characteristics of the Scattering of Sound in a Turbulent Atmosphere," Akust Zh 7, p 457-461, 1961 (English translation from Soviet Physical Acoustics, v 7, p 370-372)

12. Kologorov, AH, "The Local Structure of Turbulence in an Incompressible Viscous Fluid for Very Large Reynolds Number," Dokl Akad, Nauk SSSR 30, p 301, 1941

$$\sigma(\theta = \pi) = 0.0077\,\lambda^{-1/3}\,\frac{C_T^2}{T^2}\,. \tag{2}$$

The scattered acoustic power that is received by a monostatic system is only a function of the temperature fluctuations in a given volume. Energy scattered in all other directions ($\theta \neq \pi$) results from the combined effect of both temperature and wind fluctuations. However, for $\theta = \pi/2$, the scattering cross section $\sigma(\pi/2)$ goes to zero. Thus there is, theoretically, no acoustic scattering at directions normal to the transmitter beam.

The equation relating transmitter power, received power, and the scattering cross section $\sigma(\theta)$ for distributed scatters in the atmosphere is (see appendix A):

$$P_r = \left[P_T \cdot E_T \cdot G'\right]\left[\frac{C\tau}{(1-\cos\theta)} \cdot \frac{A_r}{R_2^2} \cdot E_r\right]\left[e^{-k(R_1+R_2)}\right]\sigma(\theta)\,, \tag{3}$$

where P_r is the received electrical power; P_T is the transmitted electrical power; E_T is the efficiency of conversion of transmitted electrical to acoustical power; G' is the gain-shaping factor for the bistatic transmitter and receiver antennas (see appendix A), τ is the pulse length; θ is the scattering angle (see equation 1); A_r is the receiving antenna area; R_2 is the distance from the scattering volume to the bistatic receiver; E_r is the effective receiving antenna aperture factor; $e^{-k(R_1+R_2)}$ is the molecular attenuation factor for the loss of power over the total propagation distance; and R_1 is the distance from the transmitter to the scattering volume.

The fundamental measurement made by the acoustic system is the signal intensity of the backscattered acoustical power in the monostatic mode, and the doppler shift in the acoustic signals in the bistatic mode. The backscattered signals reveal the vertical organization of the thermal-mixing regions of the lower atmosphere. In the bistatic mode, the doppler shift of the scattered acoustic signals from the observed region is used to calculate the three orthogonal components of the total wind vector.

The bistatic configuration for determining the doppler shift in the acoustic signals is shown in figure 1. The transmitter antenna forms a conical beam into which pulses of acoustic energy are transmitted. A bistatic fan-beam receiver antenna continuously views a large range interval along the transmitted beam, and scattered acoustical energy from the scattering volume arrives at the receiver antenna at an elevation angle ϕ. The doppler shift in the received signal is then proportional to the component of the wind along the scattering vector $\vec{q}$ which bisects the angle formed between the scattering vector $\vec{K}_s$ and $-\vec{K}_o$. The wind velocity component along $\vec{q}$ is:

$$\vec{V}_q = \left(\frac{f_d}{f}\right)\left(\frac{C}{2}\right)\left(\sin\frac{\theta}{2}\right)^{-1}\,, \tag{4}$$

where f_d is the doppler shifted acoustic signal and f is the transmitted frequency. When using three bistatic receivers in a configuration as shown in figure 2, the three measured velocity components (equation 4) corresponding to antennas 1, 2, and 3 (ie, $\vec{V}_1$, $\vec{V}_2$, and $\vec{V}_3$) are used to calculate unambiguously the three orthogonal velocity vector components of the wind field for a given range cell. Processing of the bistatically received signals as a function of time-of-arrival after the transmitted pulse, determined by the geometrical configuration and velocity

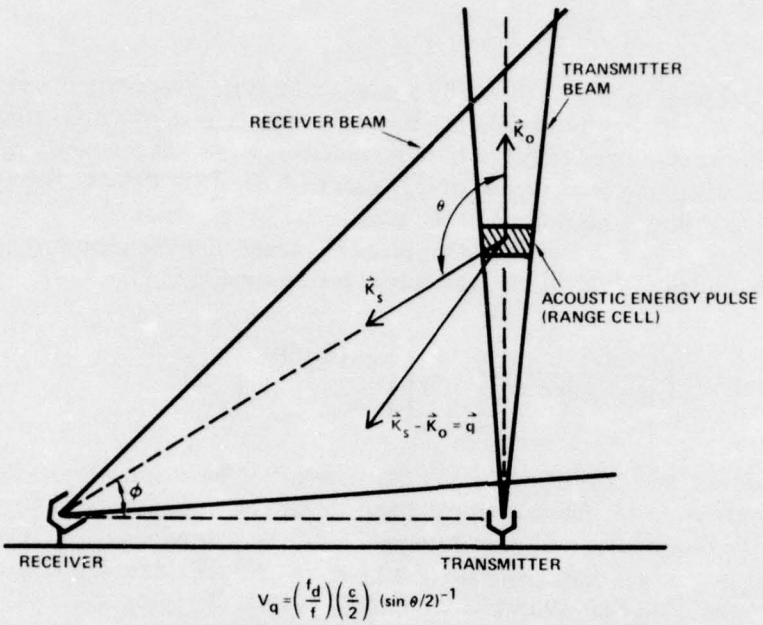

Figure 1. Basic configuration of the wind-measuring system for determining doppler shifts in acoustic signals.

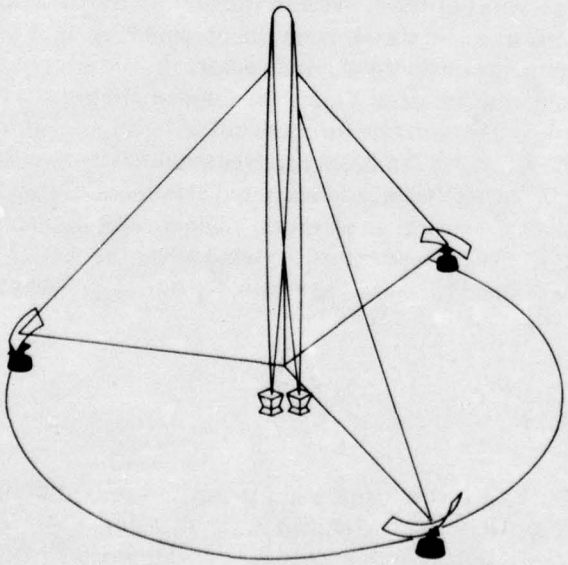

Figure 2. Bistatic and monostatic antenna configuration for the acoustic echosounder and wind-sensor system.

of sound, gives the three orthogonal wind components as a function of altitude for each pulse. Height intervals for which wind measurements can be made, are determined by the baseline distances (transmitter to bistatic receiver baselegs) and the vertical fan-beam pattern.

Good signal-to-noise ratios (S/N) must be insured for efficient acoustic wind-sensor measurements. One limitation to the fan-beam receiving antenna is that the fan beam receives the background acoustic noise over the entire fanned area while sensing doppler-shifted signals from only the small pulse-illuminated volume. Consequently, strong acoustic signals are required to obtain the same S/N as for narrow beamwidth receiving antennas. This represents a particular problem for echoes from higher elevations which are weaker because of the greater distance but which still must compete against strong surface noise received simultaneously. Therefore, instead of using a fan-beam antenna configuration in a noisy environment, either a vertically scanned pencil beam, synthesized by a phased transducer array, or a multiple array of vertically stacked, electronically switched, narrow beams should be used to track the pulse for improved S/N.

SOUNDER CONFIGURATION AND OPERATION

The geometrical configuration of the XONICS (ref 13) acoustic echosounder and wind-sensor system at NELC, Point Loma, is shown in figure 3. The bistatic receivers 1, 2, and 3 are located at elevations of 38, 107, and 117 metres above mean sea level, and at distances of 419, 483, and 468 metres, respectively, from the colocated transmitter and monostatic receiver (located at 104 metres above mean sea level) and at angles $\theta_{12}, \theta_{23}, \theta_{31}$ of approximately 120^{o} (terrain constraints prevented selection of identical base legs). The observable height window of the wind sensor system is from 80 to 575 metres above ground. For this geometry, the scattering angle θ (equation 1) varies between 98 and 147^{o}.

The acoustic-sounder transmitter uses a 3-by-3 loudspeaker array (Altec 288C drivers). The transmitting array operates at 2015 Hz and has a specified 6.5^{o} beam from its 1.22m square aperture which is surrounded by a double-walled acoustic shield to minimize side-lobe effects. The total electrical input power to the nine-element array is 1350 watts with a specified electro-acoustic conversion efficiency of 27 percent (radiated power of 365 acoustical watts). The pulse length is selectable at 10, 50, or 200 msec and the pulse-repetition interval (pri) is variable.

The receiving antennas consist of acoustically shielded 1.68m paraboloidal dishes with adjustable microphone-feedhorn assemblies. The microphones are Sennheiser MKH 450 cardioid types. The feedhorns for the three bistatic receivers provide the vertical fan-beam coverage by employing a long conical horn of rectangular cross section and a single microphone at the apex. The azimuthal beamwidth is 6.5^{o} and the vertical beamwidth is 36^{o}. The monostatic antenna uses a simple conical feedhorn All feedhorns are positioned such that the mouth of the horn is in the focal plane of the dish. All receiver antenna cavities are double-walled and acoustically shielded to minimize side lobes and resulting interference from spurious noise and direct feedthrough. The receiving cavities are environmentally sealed to protect the microphone and dish by an acoustically-transparent Tedlar window over the antenna aperture. The effective bistatic antenna aperture is 58 percent of the geometrical area of the dish. Figure 4 shows the colocated transmitter and monostatic receiver and figure 5 shows a bistatic receiver. The transmitter power amplifiers and receiver preamplifiers are housed in

13. XONICS Inc, Technical Manual and Software Description for the NELC Wind Sensor System, TR-50, March 1974

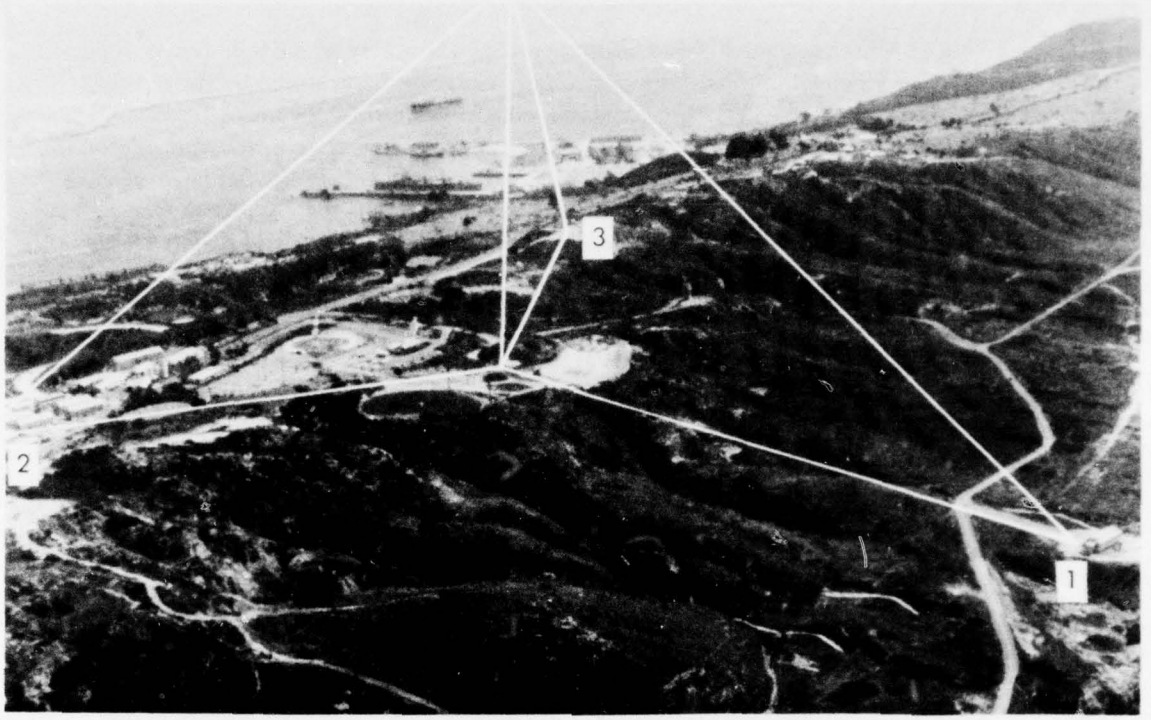

Figure 3. Geometrical configuration of the XONICS acoustic echosounder and wind-sensor system at NELC.

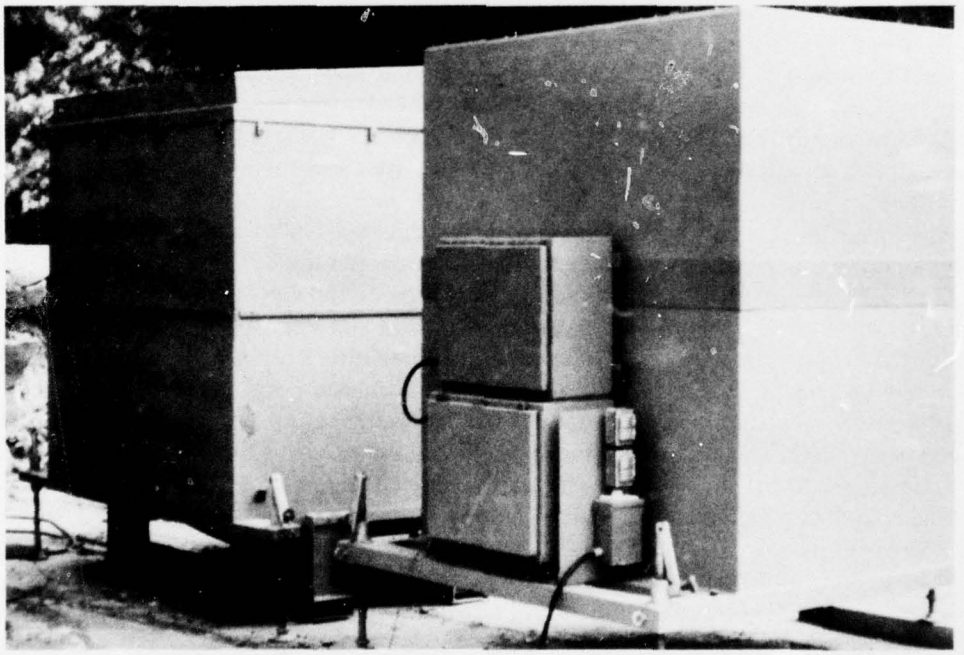

Figure 4. Colocated antenna cavities for the acoustic transmitter and monostatic receiver.

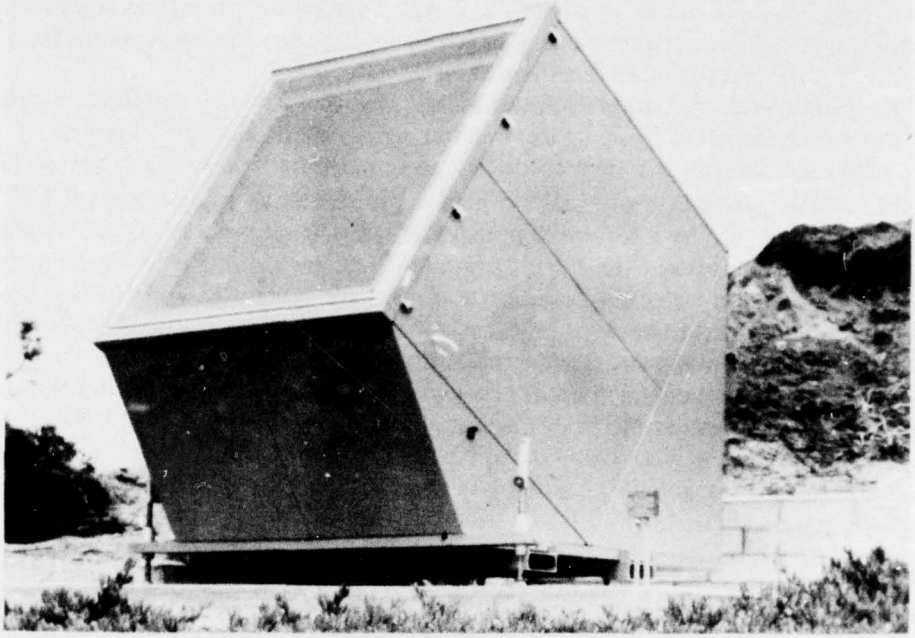

Figure 5. Fan-beam antenna cavity for the acoustic bistatic receiver.

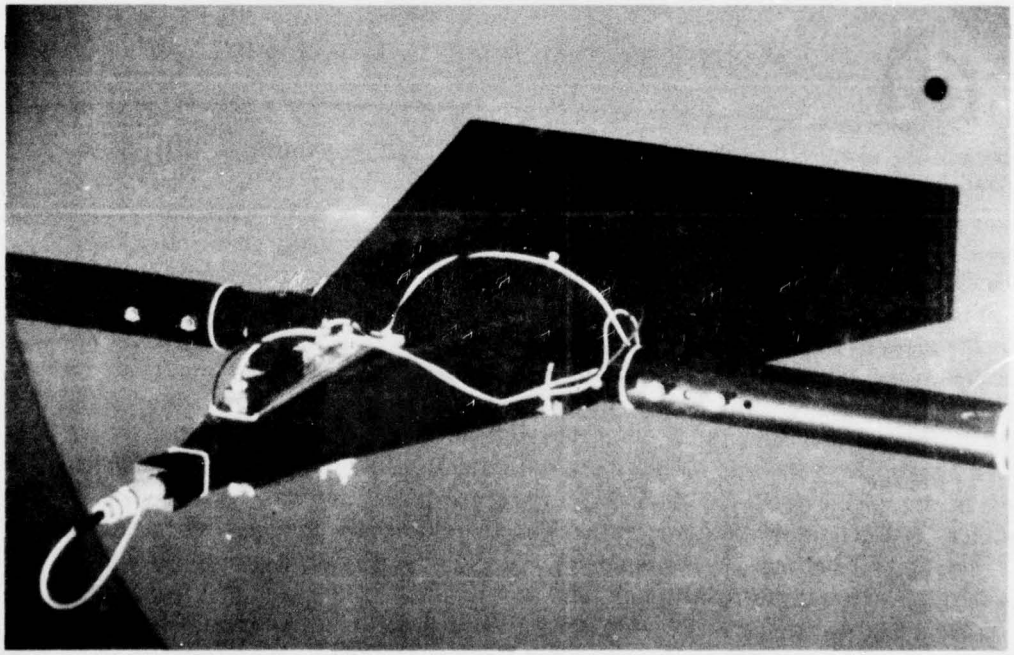

Figure 6. Microphone/feedhorn assembly for the bistatic fan-beam receiver antennas.

water-proof cavity-mounted enclosures. Each cavity is mounted on screw jacks to provide leveling adjustments for proper antenna alignment. Figure 6 shows the microphone/feed-horn assembly for the bistatic receiver antennas.

The central control for the transmitter pulse-generating circuitry and data-processing hardware/software is shown in figure 7. Backscatter signals are displayed on intensity-modulated cathode-ray tubes and are recorded by 35-mm, shutterless, movie cameras. The bistatic, doppler-shifted, acoustic signals are sampled in proper timing sequence by an A/D converter and are processed by a Nova 820 minicomputer. Digital processing of the bistatic signals includes data acquisition from the proper antenna at the proper range gate, transformation to a doppler spectrum using fast Fourier transforms, averaging over some specified time interval, estimation of signal-to-noise ratio, calculation of wind components corresponding to the doppler-shifted frequencies, and outputting of the corresponding wind profiles using a teletypewriter. Functionally, the minicomputer provides the executive control for the wind-sensor operation which includes PRI and triggering control, input control of raw data to the processor, and output of the processed data to the teletypewriter. Figure 8 shows the input and output data formats for the acoustic wind-sensor program. The input parameters required by the computer program are defined in this figure. The output velocity components, V_X, V_Y, and V_Z, are calculated for each of the height intervals. V_X and V_Y are the orthogonal horizontal-velocity components and are positive in the easterly and northerly direction, respectively. V_Z is the vertical component and is positive in the upward direction. The averaging time is determined by the transmitter PRI and the number of incoherent spectra to be averaged which are input parameters to the computer. Completion time of the averaging period is given in the output.

ACOUSTIC ECHOSOUNDER OBSERVATIONS

Examples of acoustic backscatter echoes which qualitatively show the temperature structure of the lower atmosphere obtained from the vertically pointing acoustic echosounder, are shown in figures 9 through 11. The record for 9 June 1974, figure 9, shows multiple echo layers at heights of 300, 450, 600, and 700 metres. The upper, horizontally-stratified echo layers indicate temperature mixing in regions normally assumed to have dynamic thermal stability. The strongest of the echo layers (layering between 250 and 350 metres) is at the base of the major temperature inversion or the top of the marine layer. This is the region where the temperature structure constant, C_T, is most likely to be largest. All of the unstructured echoes below about 250 metres are thought to be created by orographically induced mechanical turbulence (forced turbulence by wind over rough terrain). Acoustic echoes which show thermally unstable conditions throughout a deep layer are shown in figure 10. Vertically oriented echoes, extending throughout the height range, are returns from temperature fluctuations produced by turbulent mixing. Figures 9 and 10 show that, for the monostatic sounder, the acoustic returns give an indication of the dynamic thermal stability, or changes in the temperature-lapse rates, characterized by mixing regions along the path of a transmitted sound pulse.

Figure 11 shows the height of the major temperature-mixing region, normally at the top of the marine layer, for a day in which the depth of the marine layer changed appreciably. The height varied from 300 metres at 1200 hours (PDT) to 700 metres at 1405 hours (PDT). By 1830 hours (PDT), the depth of the marine layer had decreased to 200 metres. These observations were taken with a 10-msec pulse length (an equivalent 1.7-metre range resolution)

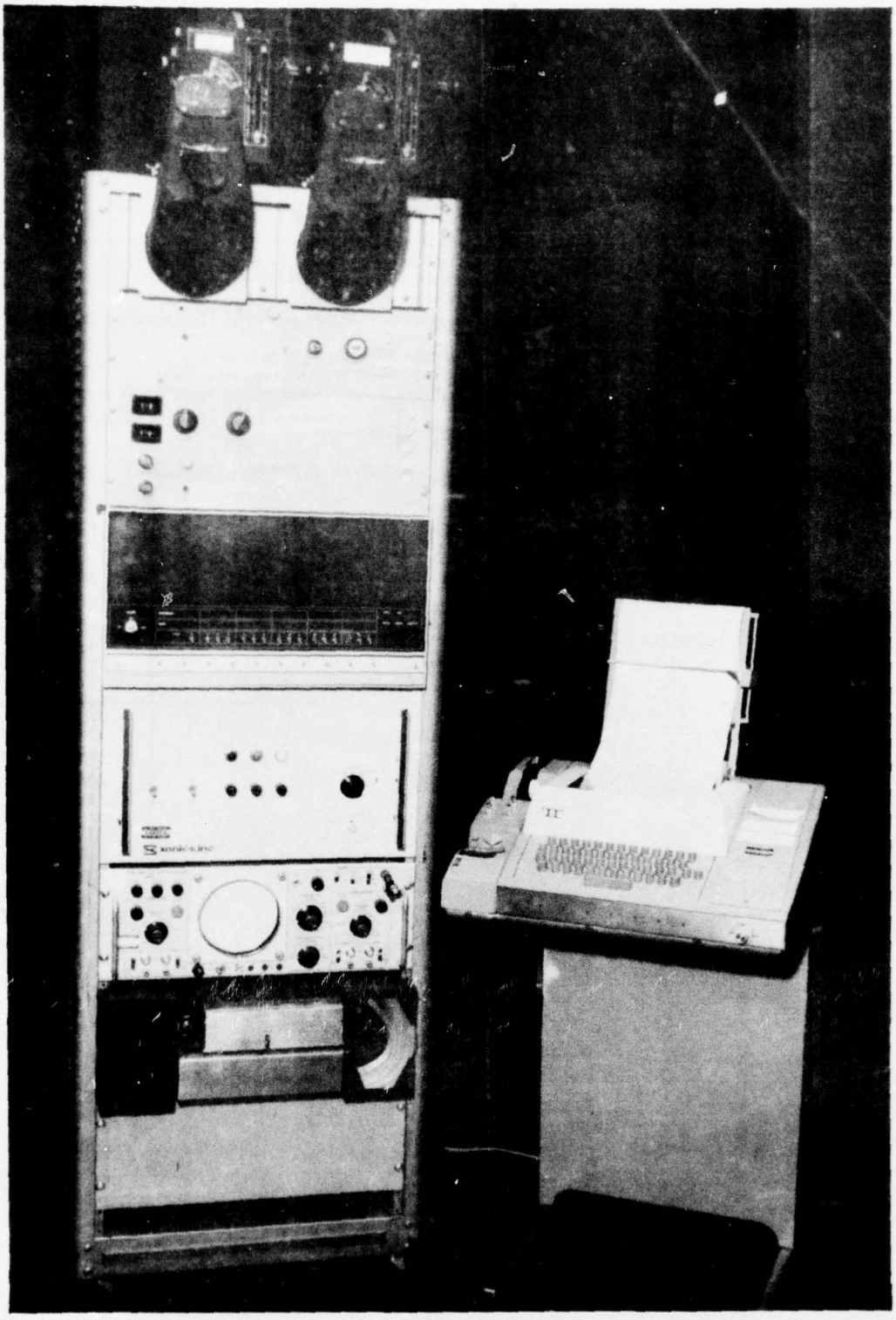

Figure 7. Input/output executive control center for the acoustic echosounder and wind-sensor system.

ACOUSTIC WIND-SENSOR PROGRAM

INPUT FORMAT

ACOUSTIC WIND SENSOR
NELC VER VI

TEMPERATURE	= 293	–	SURFACE TEMPERATURE (K)
HMIN	= 125	–	MINIMUM HEIGHT WINDOW (m)
HMAX	= 665	–	MAXIMUM HEIGHT WINDOW (m)
ALT INCREMENT	= 60	–	WINDOW HEIGHT (m)
NO RNG GATES	= 10	–	NUMBER OF RANGE GATES BETWEEN HMAX AND HMIN
XMTR PRI	= 6000	–	PRI IN msec
XMTR FREQ	= 2015	–	TRANSMITTER FREQUENCY (Hz)
PULSE LENGTH	= 200	–	TRANSMITTER PULSE LENGTH (msec)
NO AVERAGES	= 10	–	NUMBER OF INCOHERENT SPECTRA TO BE AVERAGED
NO SAMPLES	= 128	–	SAMPLING CRITERIA
SAMPLE FREQ	= 620		
SAMPLE TIME	= 206		
CYCLE TIME	= 5	–	TIME IN MINUTES BETWEEN AVERAGES

OUTPUT FORMAT

DATE = 08/18/75
TIME = 19:43:00

ALT METRES	VX M/SEC	VY M/SEC	VZ M/SEC
125	+1.9	−2.4	+0.6
185	+1.8	−2.6	+0.3
245	+0.7	−1.6	+0.1
305	−0.3	+0.0	+0.3
365	−0.7	+0.5	−0.0
425	−2.7	+1.1	+0.4
485	−3.4	−1.4	+0.9
545	−1.1	−0.7	+0.5
605	+11.0	+15.3 B	−3.0 B
665	−8.4	−10.2	+4.6 B

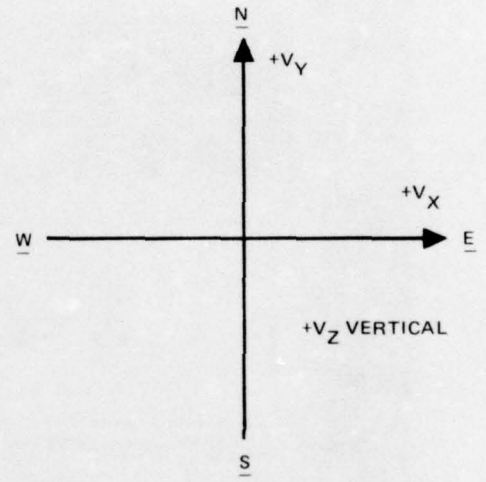

Figure 8. Input/output data format for the acoustic wind-sensor program.

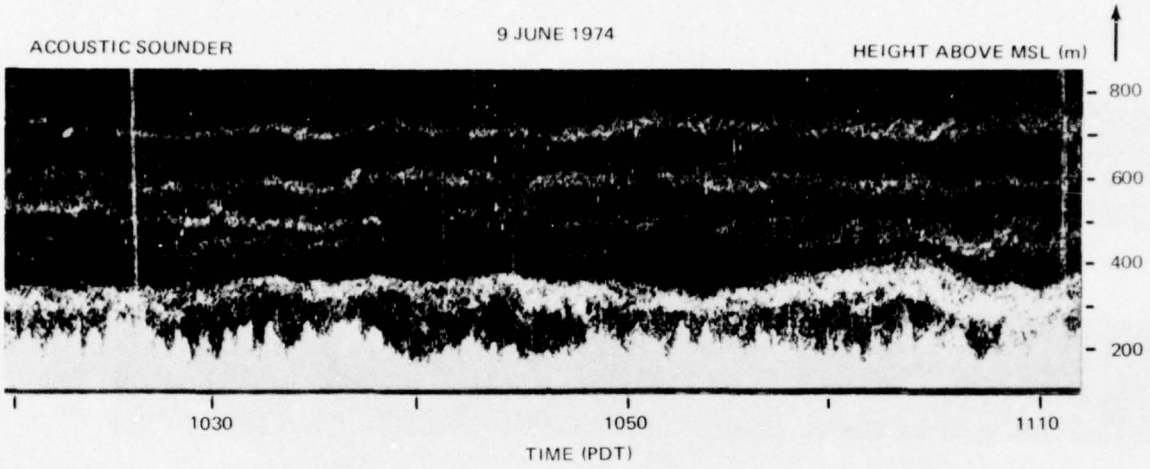

Figure 9. Acoustic-echo structure for 9 June 1974 showing multiple-echo layer structures.

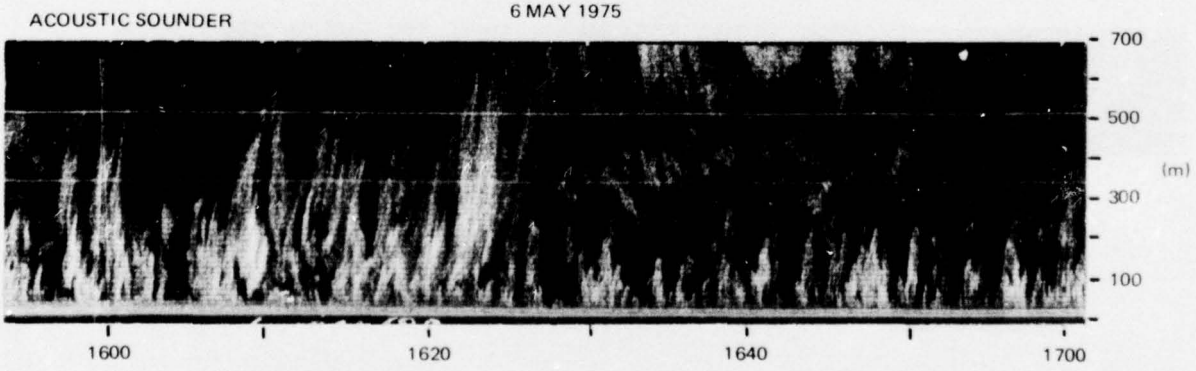

Figure 10. Acoustic-echo structure for 6 May 1975 showing thermally unstable conditions.

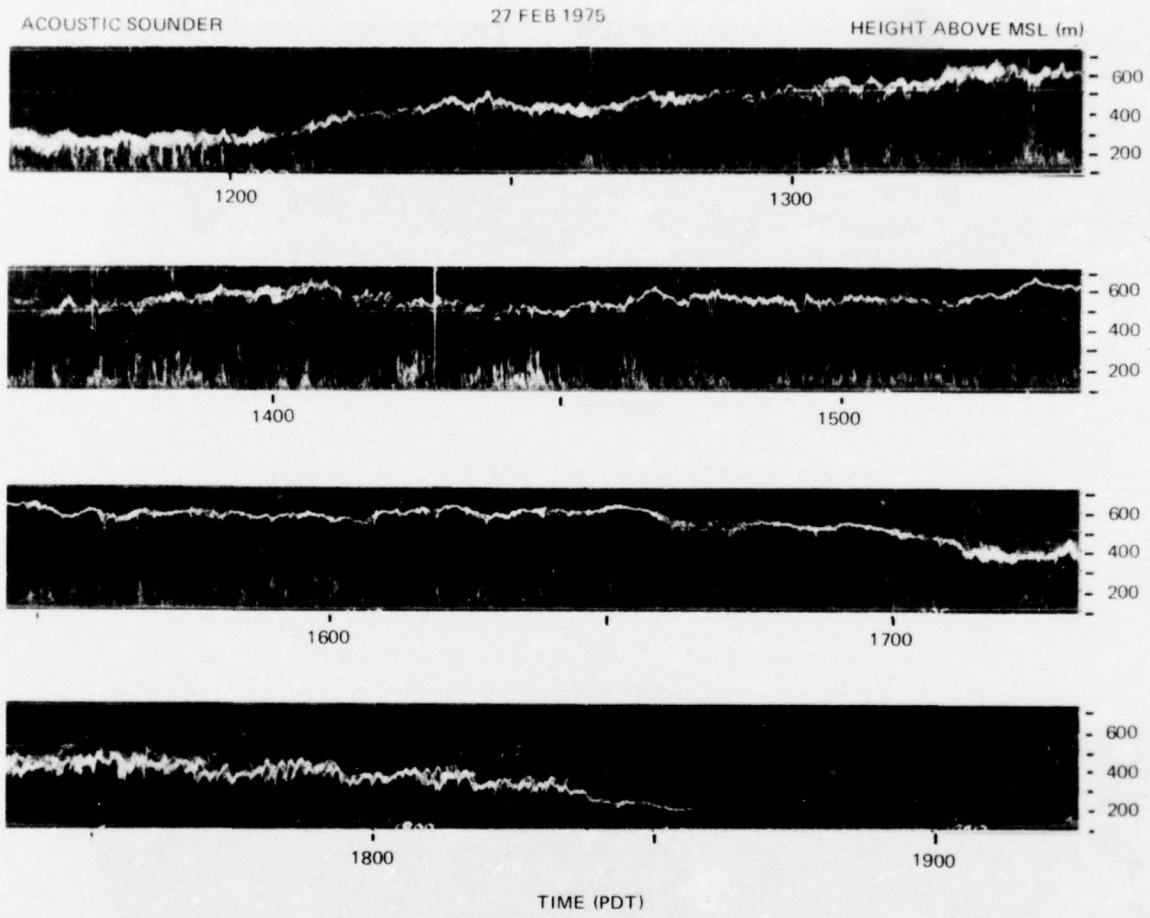

Figure 11. Acoustic-echo structure for 27 Feb 1975 showing the depth of the marine layer as a function of time.

while those shown in figure 9 were taken with a 200-msec pulse length (34-metre range resolution). Differences in the structural details in the layers, shown in figures 9 and 11, illustrate the effects of range resolution on the ability to observe atmospheric microstructure. If the record, figure 11, had been taken with the coarser resolution (eg, 34 metres) the microstructural details of the layers would most likely be similar to those of figure 9.

Simultaneous acoustic echosounder and FM-CW radar observations of atmospheric structure are shown in figures 12 and 13. These two sounding techniques are complementary to each other because the microwave radar primarily senses moisture fluctuations whereas the acoustic sounder senses temperature fluctuations. Since these two remote sensors are sensitive to two different atmospheric parameters, simultaneous observations might be expected to show similarities and differences in the height variation depending upon whether temperature and moisture fluctuations follow the same mixing process.

Figure 12 is an example where both the acoustic sounder and FM-CW radar sensed echo returns from the same height region. The echo type observed by the FM-CW radar (lower part of fig 12) has been classified as an S-echo and is identified as returns normally near cloud tops (ref 14, 15). Surface observations taken at North Island (located approximately 5.3 km inland) on 22 December 1974 at 0100 hours (PDT), showed overcast conditions with a cloud base at 335 metres. Therefore, there appear to be sufficient humidity and temperature fluctuations at the boundary between the lower, moist, cooler air and the upper, warmer, drier air to yield acoustic-sounder and FM-CW radar returns. The acoustic-echo structures between the cloud-top echoes and 200 metres are probably returns from weak, thermally unstable regions. Corresponding echo structures were not observed by the FM-CW radar. Acoustic echoes below 200 metres are probably caused by temperature fluctuations resulting from orographically induced mixing.

Acoustic-sounder and FM-CW radar echoes from horizontally stratified layers often contain evidence of organized wave structures whenever the region near the layer is stable (ref 16 through 19). Figure 13 shows an example of stable internal wave structures simultaneously observed by the acoustic and microwave remote sensors. The acoustic-sounder record shows echoes from stratified multiple layering (at least three layers) upon which internal wave motions are superimposed. In contrast to the acoustic records, the FM-CW radar revealed only wave motions in the two echo layers below about 280 metres and the intensity of these echoes was not as high. The bright horizontal lines represent range markers and clutter from fixed ground targets. The wave period for both sensors ranges from 5 to 7 minutes with crest-

---

14. Naval Electronics Laboratory Center Technical Report 1849, Simultaneous FM-CW Radar and Lidar Probing of the Atmosphere, by VR Noonkester, DR Jensen, and JH Richter, 1 November 1972
15. Naval Electronics Laboratory Center Technical Report 1862, Meteorological Processes and FM-CW Radar Soundings in the Boundary Layer, by VR Noonkester, DR Jensen, and JH Richter, 5 February 1973
16. Hall, FF, Jr, "Temperature and Wind Structure Studies by Acoustic Echo-Sounding," Remote Sensing of the Troposphere, (VE Derr, editor), National Oceanic and Atmospheric Administration, p 18-1 to 18-25, August 1972
17. Gossard, EE, JH Richter, and D Atlas, "Internal Waves in the Atmosphere from High-Resolution Radar Measurements," Journal of Geophysical Research, v 75, no 18, p 3523-3536, June 1970
18. Beran, DW and FF Jall, Jr, "Remote Sensing Applications in Air-Pollution Meteorology," Second Joint Conference on Sensing of Environmental Pollutants (reprint), p 231-246, Instrument Society of America, December 1973
19. Hooke, WH, JM Young, and DW Bean, "Atmospheric Waves Observed in the Planetary Boundary Layer Using an Acoustic Sounder and a Microbarography Array," Boundary Layer Meteorology, v 2, p 371-380, 1972

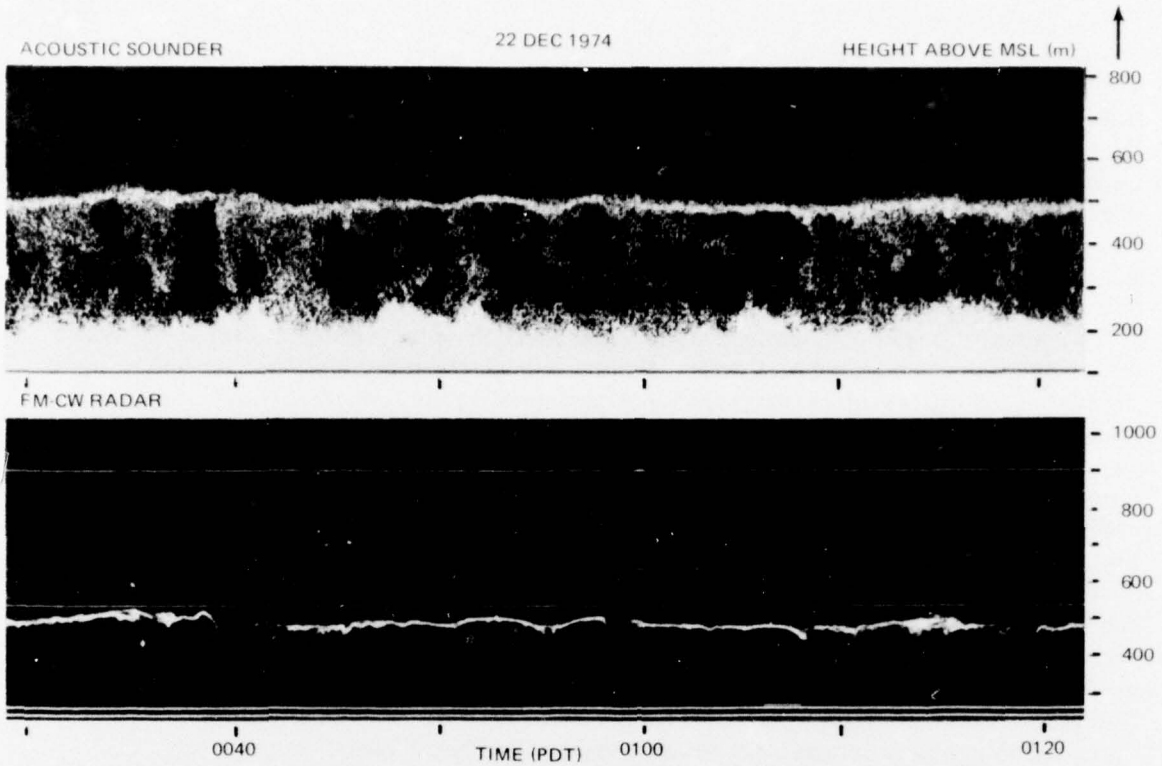

Figure 12. Simultaneous acoustic-echo and FM-CW radar observations of cloud tops (S-echoes) for 22 Dec 1974.

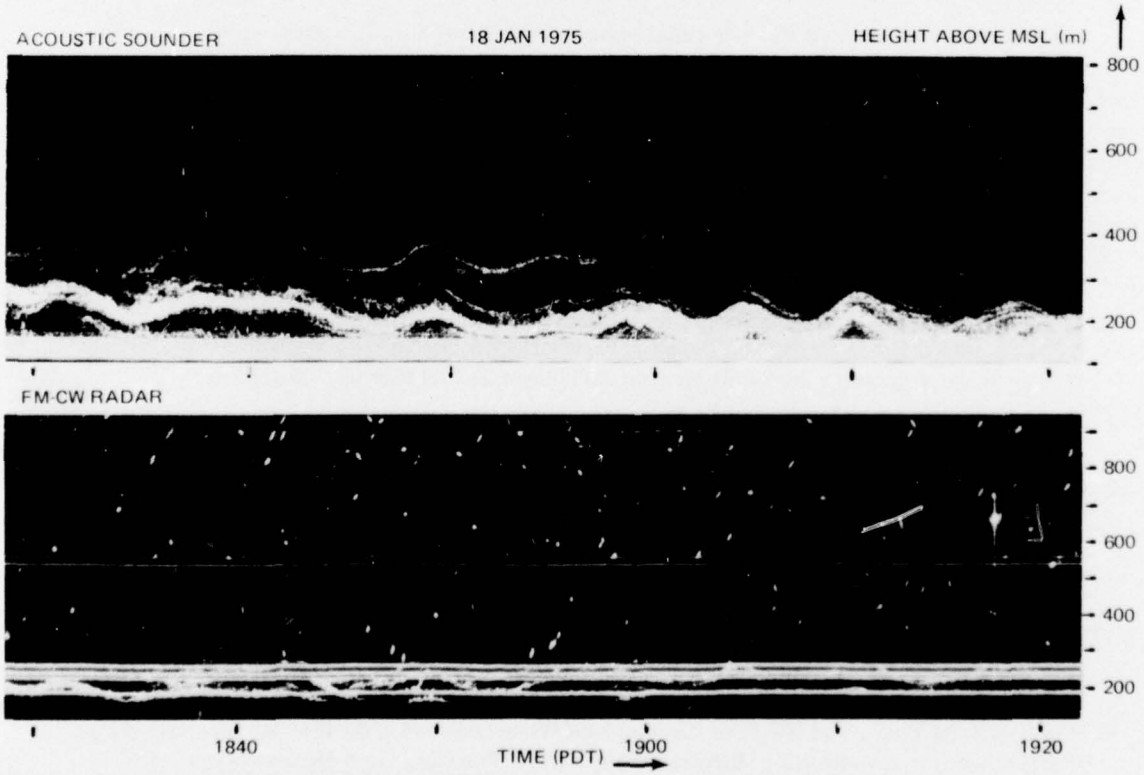

Figure 13. Simultaneous acoustic-echo and FM-CW radar observations of internal wave structures for 18 Jan 1975.

to-trough amplitudes up to 80 metres. A rawinsonde taken at 1700 hours (PDT) on this day at Montgomery Field in San Diego (MFY) (located about 17 km NE of the sounders) shows a temperature inversion from 200 to 280 metres with nearly isothermal conditions above up to 500 metres. The most intense echoes for both sounders occurred in the height region of the temperature inversion (200 to 280 m), while the weaker acoustic echo (centered at 350 m) occurred within the nearly isothermal regions above the inversion. Dot echoes on the FM-CW radar record are returns from insects. The differences in the observed vertical depth of field may be an indication that the region of temperature mixing is vertically deeper than the region of moisture mixing.

An example of simultaneous observations which show the complementary nature of the two sounders for interpreting the marine layer is shown in figure 14. This record, analyzed by Richter and Jensen (ref 20), shows a Kelvin-Helmholtz (K-H) instability observed by the acoustic sounder to be below the multiple undulating echo layers observed by the FM-CW radar (traced by solid and dashed lines, respectively, in the lower part of figure 14). The nonbreaking wave observed by the FM-CW radar shows some evidence of downward streamers or plume ejections from the troughs of the lowest layer. As discussed by Richter and Jensen (ref 20) this may be revealing entrainment of air from above by K-H waves whose vertical amplitude was sufficient to influence overlying regions and entrain moisture into the troughs of the K-H waves below this layer. From independent FM-CW radar observations, Gossard et al (ref 21), suggested that the streamers or plume ejections observed on the undulating layers may have been caused by self-induced reduction of Richardson's number together with wind shear in the medium. However, the simultaneous observations of the acoustic sounder and the FM-CW radar offer an alternate explanation through the ability to sense moisture and temperature fluctuations separately.

ACOUSTIC WIND-SENSOR EVALUATION AND OBSERVATIONS

Curves which show the expected ranges of received acoustic power of echo intensities at a bistatic receiver as a function of height above the transmitter for different atmospheric conditions, are shown in figure 15. The curves labeled $P_{r\,(min)}$ and $P_{r\,(max)}$ are calculated minimum and maximum expected acoustic power that would be received for high and low values of the structure constants C_T and C_V. The P_r curves were calculated from equation (3) for P_T = 1350 electrical watts, pulse length of 200 msec, k = 0.0015 m^{-1} (molecular attenuation coefficient for acoustics) (ref 7), an assumed gain-shaping factor for the bistatic antenna configuration of 0.24 (see appendix A), and for a bistatic base leg of 419 metres (bistatic antenna number 1, fig 3). The measured background acoustic-noise band and the minimum detectable signal for the system are also shown in figure 15. The noise band shows the maximum and minimum values of the measured noise power for daytime and nighttime, ambient background noise measurements.

Comparison of the minimum expected power return curve, $P_{r(min)}$, and the minimum detectable signal (labeled MIN DET SIG, fig 15) shows that, for conditions of minimum C_V and C_T, acoustic signals could only be detected by the bistatic system in the height region

20. Richter, JH and DR Jensen, "Simultaneous Acoustic Sounder and FM-CW Radar Observations," p 282-289, 16th Radar Meteorology Conference (preprint), American Meteorological Society, April 1975

21. Gossard, EE, JH Richter, and DR Jensen, "Effect of Wind Shear on Atmosphere Wave Instabilities Revealed by FM-CW Radar Observations," Boundary Layer Meteorology, v 4, p 113-131, 1973

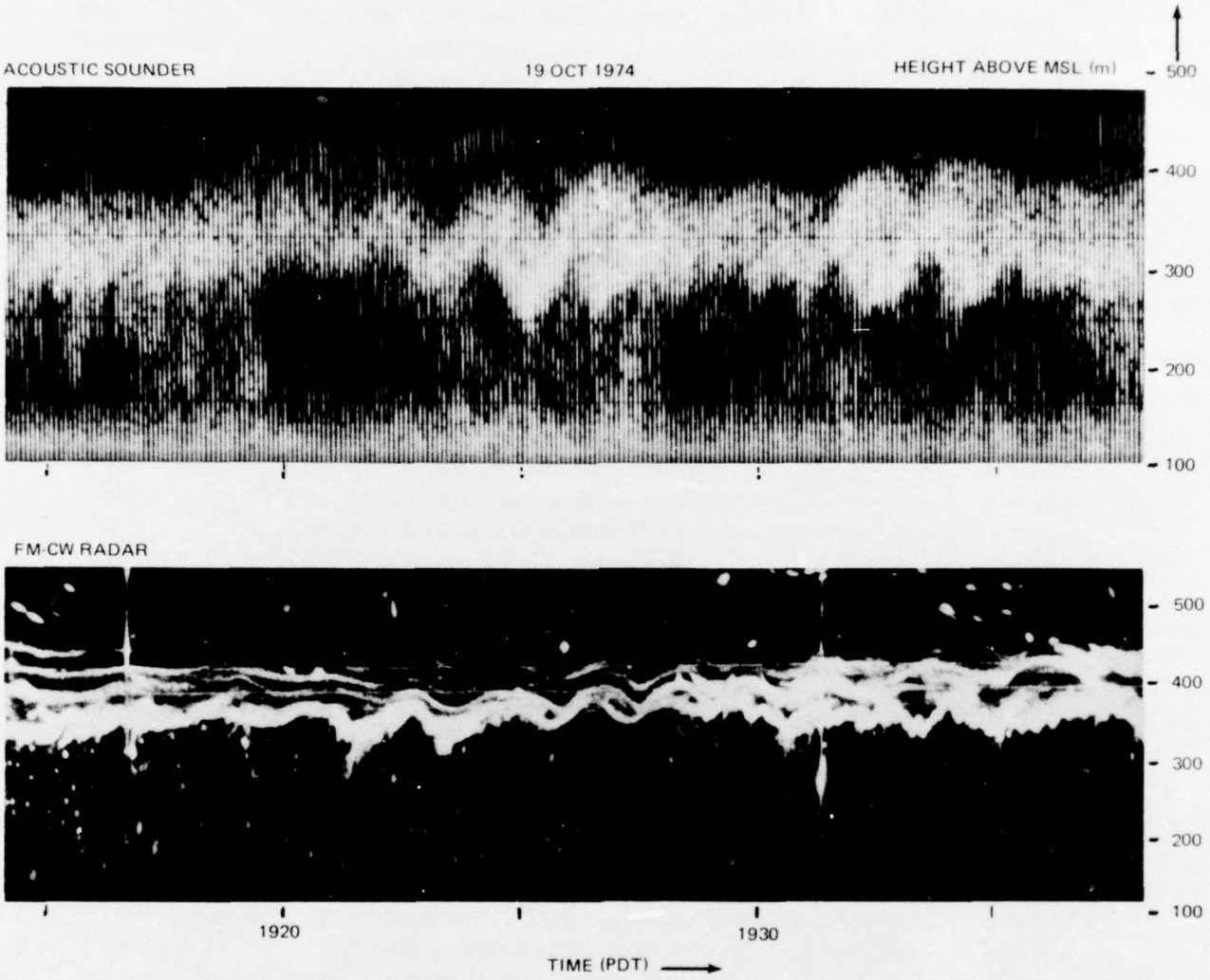

Figure 14. Simultaneous acoustic-echo and FM-CW radar observations of wave structures.

up to 350 metres. Comparison of the expected power return, $P_{r(max)}$, for enhanced values of C_V and C_T and the measured noise band, shows that consistently usable signals would be expected in the height region from 0 to 550 metres. This analysis shows that there would be sufficient signal-to-noise (area bounded between the noise band and the $P_{r(max)}$ curve) to permit reliable wind-profile calculations (provided that atmospheric noise is independent of C_V) only for conditions characterized by large C_T and C_V values.

An increase in the signal-to-noise ratio can be realized by reducing the distance between the bistatic receiver and transmitter. However, as seen in figure 3, the observable height window is reduced as the base leg is shortened. This reduces the total propagation distance (the distance from the transmitter to the scattering volume and to the bistatic receiver) and, thus, the total attenuation of the acoustic signals. The expected power curves when the transmitter and receiver are at the same elevation and separated by 200 metres (all other geometrical and operational parameters the same as in fig 15) are shown in figure 16. The position of the measured noise band, relative to the $P_{r(min)}$ and $P_{r(max)}$ curves, shows that reliable wind measurements are more likely than for longer base legs but again only for the higher values of C_V and C_T.

The principal limitation of the acoustic wind-sensor system is the poor signal-to-noise ratio believed to result from the wide receiving aperture of the bistatic fan-beam receivers. Additional noise for the above-ground receiver antenna is wind-generated by turbulent flow over the cavities. This wind-generated noise, coupled with that noise from possible vibration of the aperture window, is additive to the atmospheric noise from the fan beam. Wind-generated noise can be reduced by placing the antennas in underground bunkers with apertures flush with the ground level (ref 7 and 22).

To reduce the cavity or locally generated noise, the bistatic receiver antenna cavities were modified by: acoustically isolating the feedhorn microphone assembly from the cavity; acoustically isolating the parabolic reflector from the cavity structure; and acoustically deadening the cavity walls. The resulting improvements to the measured noise powers are shown in figure 17 for bistatic receiver 1 using the same parameters as in figure 15. The ranges for the measured noise powers for day and night are indicated at the top of figure 17. During the daytime and nighttime hours when manmade and natural background noise levels are small, sufficient signal-to-noise ratios permit reliable wind-profile determinations. However, when the noise levels are not low, daytime wind measurements are not feasible and nighttime measurements are only feasible when strong bistatic echoes are present.

Figure 18 shows the expected power curves and the measured noise band for the acoustic sounder system when the transmitter and bistatic receiver are assumed to be on the same plane and separated by 200 metres. These curves show that the signal-to-noise ratio is increased sufficiently to allow reliable nighttime and limited daytime wind measurements when base legs of 200 metres are used. However, when the length of the base leg is reduced to this dimension, the observable height window is reduced to the region below 275 metres. This reduced window seriously limits the use of the acoustic wind sensor for wind-shear studies of the Southern California coastal inversions. Comparisons of figures 15 and 17,

---

22. Willmarth, BC, EH Brown, JT Priestly, and DW Beran, "Beam Pattern Measurements for Large Acoustic Antennas," 16th Radar Meteorology Conference (preprints), p 278-281, American Meteorological Society, April 1975

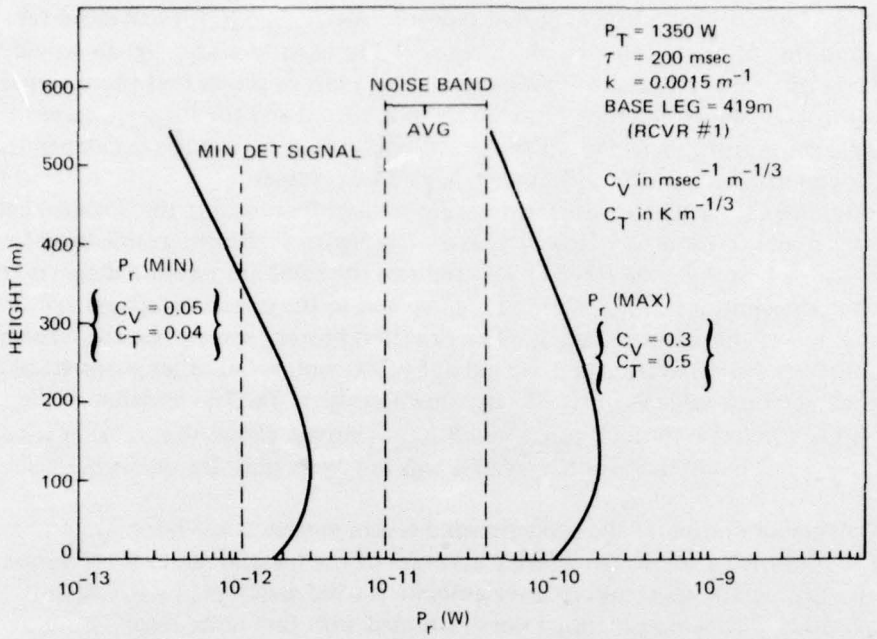

Figure 15. Power curves showing expected ranges of received acoustic power as a function of height for different atmospheric conditions. System as originally configured (see text).

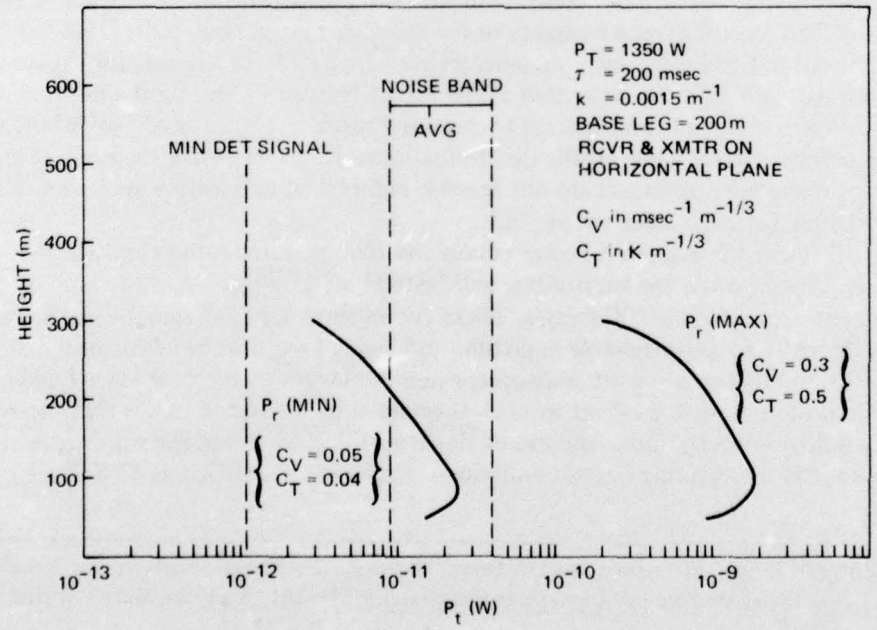

Figure 16. Acoustic wind-sensor power curves obtained using an assumed base leg of 200 metres (all other conditions the same as in figure 15).

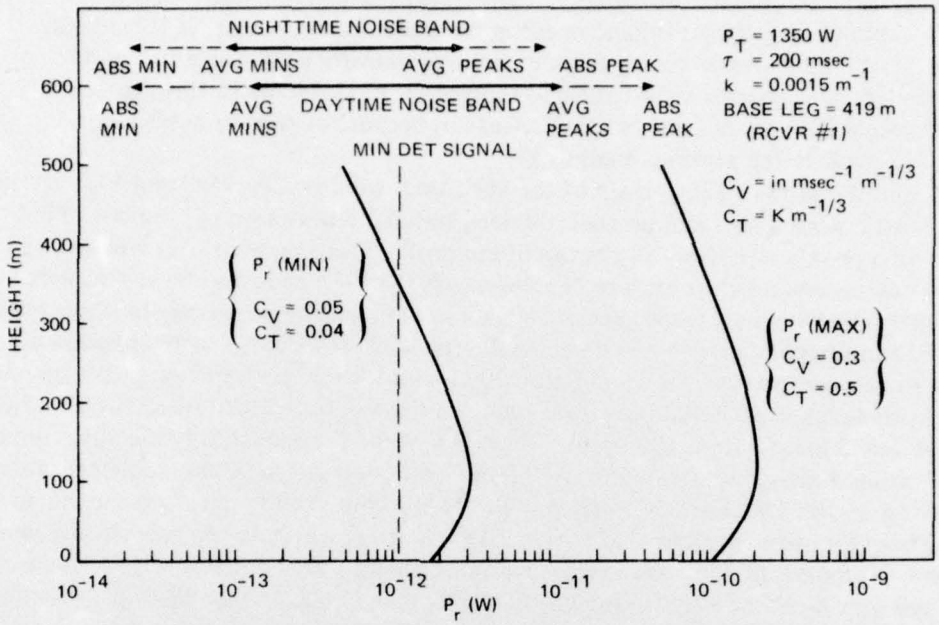

Figure 17. Acoustic wind-sensor power curves taken under conditions of figure 15 except for acoustical modifications to the bistatic fan-beam receiver antenna cavities. Measured daytime and nighttime noise bands are shown.

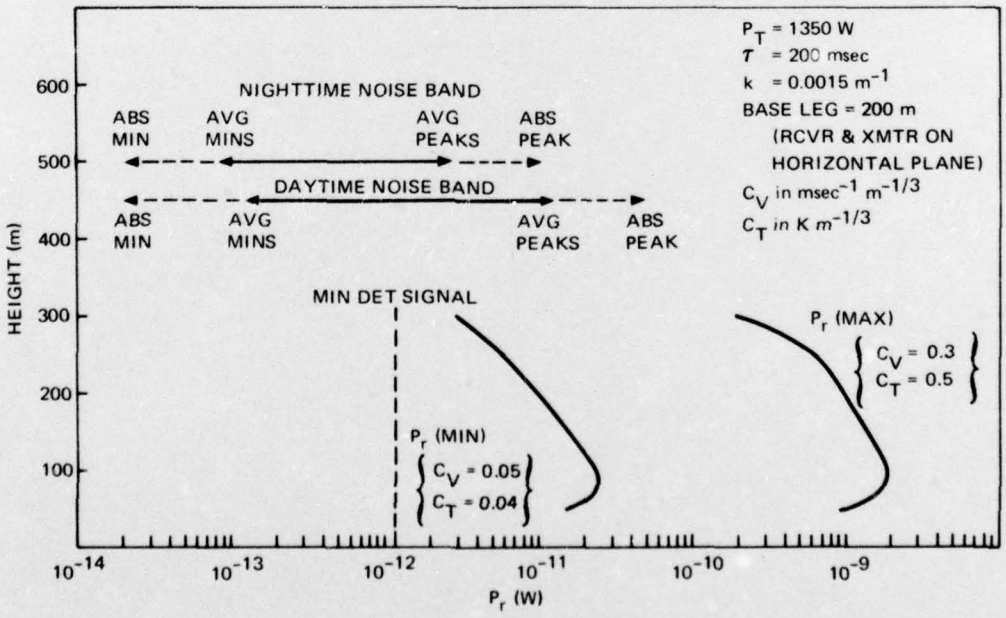

Figure 18. Acoustic wind-sensor power curves using an assumed base leg of 200 metres (all other conditions the same as in figure 17).

and of 16 and 18, show that reasonable system modification, including acoustically redesigning of the bistatic receiver antenna cavities and reduction of the base leg distances, produced significant improvement in the signal-to-noise ratio. It is believed, therefore, that the fan-beam receiving antennas are principally responsible for limitations of the antenna system. (The calculated curves for P_r in figures 15 through 18 differ somewhat from a similar presentation (ref 23) because of some simplifying assumptions made in the previous analysis.)

Figure 19 shows a comparison of the horizontal wind profiles (V_X and V_Y) measured by the acoustic wind sensor and profiles obtained simultaneously by a rawinsonde. Each acoustic wind profile represents an average of ten profile measurements over a period of 1 minute. The rawinsonde release time was 2155 hours (PDT). The acoustic and rawinsonde measurements of the winds are in general agreement. Some differences may be expected if the spatial and temporal differences between the two sensing techniques are considered. Another similar comparison, shown in figure 20, does not show good measurement agreement. The rawinsonde taken at 2050 hours (PDT) showed the V_X component of the wind to be approximately 3 $msec^{-1}$ from 100 up to 500 metres, while the acoustically measured winds increased from 3 $msec^{-1}$ at 310 metres to 9.5 $msec^{-1}$ at 480 metres. Reasonable agreement in V_X did exist up to 310 metres. Comparison of the V_Y components shows no agreement.

These comparisons show that the question of agreement between acoustically measured winds and those measured by rawinsondes has not been answered conclusively for the wind-sensing system which was tested. Good agreement can only occur when the signal-to-noise ratio is large and strong acoustic scattering exists. As shown by the expected power curves of figure 17, wind measurements are only feasible with the presently configured system during nighttime hours under selected conditions when ambient noise is low and C_T and C_V values are large. It is impossible to specify times when C_T and C_V are large and when the background noise levels are low. Thus, the use of the existing wind-sensor system has serious limitations.

23. Richter, JH and DR Jensen, "New Developments in the Detection of Atmospheric Structures," Proceedings of the NATO Advanced Study Institute on Atmospheric Effects on Target Identification and Classification, Goslar, Germany, (in press)

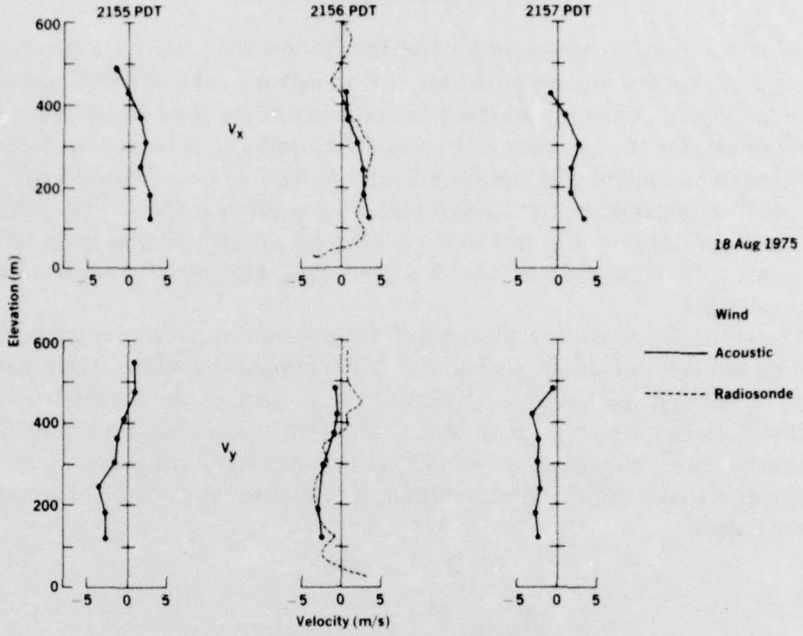

Figure 19. Horizontal wind profiles measured by acoustic methods (solid line) and by rawinsonde tracking (dashed line) for 18 Aug 1975.

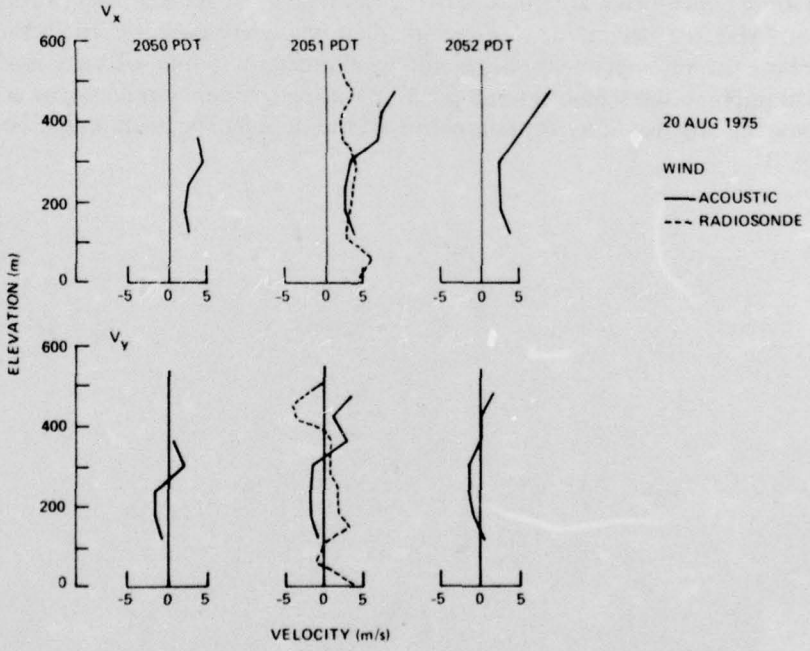

Figure 20. Horizontal wind profiles measured by acoustic methods (solid line) and by rawinsonde tracking (dashed line) for 20 Aug 1975.

CONCLUSIONS

Acoustic sounders represent a powerful tool for the investigation and study of the temperature and wind structure of the lower troposphere. The XONICS acoustic sounder has the capability of measuring all three components of the total wind vector and, simultaneously, measuring the intensity of backscattered echoes. However, with the presently configured system, limited wind measurements are feasible only for selected conditions during nighttime hours when the background noise is low and C_T and C_V values are large. The principal limiting factor in this acoustic wind-sensor system appears to be the poor signal-to-noise ratio obtained with above-ground, fan-beam, bistatic receiving antennas. (See Appendix B.)

The vertically pointing echosounder permits continuous monitoring of the vertical temperature structure of the troposphere with high range resolution. Observations give an indication of the dynamic thermal stability along the path of the transmitted sound pulse. Observed structures include layering, waves, cloud-top echoes, Kelvin-Helmholtz instabilities, and turbulence. The acoustic-sounder returns are highly complementary to the microwave radar returns used in the interpretation of refractive phenomena observed by microwave radars.

RECOMMENDATIONS

To improve the operational capability of the XONICS wind-sensor system, a significant improvement in the signal-to-noise ratio must be obtained. Noise reduction appears possible using pencil-beam antennas (either phased-array or stacked, electronically-scanned antennas). Also, by placing the receiver antennas below ground level, the noise caused by wind striking the antenna enclosures would be eliminated. Some software modification might also improve the signal-to-noise ratio. By using frequency-tracking or cross-correlation techniques, the impulse-noise contamination of the doppler spectrum might be reduced (see Appendix B).

APPENDIX A: DEVELOPMENT OF THE ACOUSTIC ECHOSOUNDING EQUATION

The development of the fundamental equation relating the transmitted power, the received power, and the scattering cross section, $\sigma(\theta)$, for acoustics is analogous to the development of the meteorological radar equation (ref 16). The basic radar equation, applied to acoustic echo sounding, gives the received echo power, P_r, in terms of transmitted power, P_T, antenna gain, G_T, the acoustic scattering cross section for distributed scatters, $\sigma(\theta)$, the effective illuminated volume, V, the effective cross section of the receiver antenna, A_r, the atmospheric attenuation, L, the range from the transmitter to the scattering volume, R_1, and the range from the scattering volume to the receiver, R_2, as:

$$P_r = \underbrace{\frac{P_T G_T}{4\pi R_1^2}}_{a} \cdot \underbrace{\frac{V\sigma(\theta)}{R_2^2}}_{b} \cdot \underbrace{A_r}_{c} \cdot \underbrace{L}_{d} . \qquad (A1)$$

The factor (a) in equation A1 gives the power density of an illuminating wave front at a range, R_1, from the transmitter. The numerator of (b) is the equivalent scattering cross section and is, by definition, the scattered power per unit incident flux into a unit solid angle. Division by R_2^2 makes (b) equal to the ratio of the power density of the scattered signal at the receiver per unit incident flux on the scattering volume. The product of (a) and (b) gives the power density of the scattered wave at the acoustic receiver. The third factor (c) is the effective receiving antenna aperture, A_r, and (d) is the atmospheric attenuation factor, L.

The development of equation A1 assumes uniform antenna gains and axially symmetric beams for both the transmitter and receiver. However, in actuality, the gain changes across the antenna aperture (both in azimuth and elevation) and the amount of power incident on the scatters within the scattering volume are dependent upon the position within the beam. To obtain quantitative information on system performance or atmospheric parameters related to scattering, it is necessary to know the gain characteristics of the transmitting and receiving antennas.

The average power, received from an illuminated volume located within the transmitter's conical beam (defined by the half angle α_o), can be found from equation A1 by substituting $G_T(\alpha_o)_{avg}$ for G_T, and $A_r D_r(\alpha_o)_{avg}$ for A_r, where $G_T(\alpha_o)_{avg}$ is the averaged gain over the conical transmitter beam (both in azimuth and elevation) and $D_r(\alpha_o)_{avg}$ is the fraction of on-axis gain for the receiver. Equation A1 then becomes:

$$P_r = \frac{P_T G_T(\alpha_o)_{avg}}{4\pi R_1^2} \cdot \frac{V\sigma(\theta)}{R_2^2} \cdot A_r D_r(\alpha_o)_{avg} \cdot L . \qquad (A2)$$

Evaluation of the acoustic echo-sounding equation A2 for a specific system requires an accurate knowledge of the antenna gain characteristics to obtain values of $G_T(\alpha_o)_{avg}$ and $D_r(\alpha_o)_{avg}$. Hall and Wescott (ref 24) have evaluated these gain parameters for a monostatic

24. Hall, FF and JW Wescott, "Acoustic Antennas for Atmospheric Echosounding," Journal of the Acoustic Society of America, v 56, no 5, p 1376-1382, November 1974

acoustic echosounder where the transmitting and receiving antennas are the same and have an antenna pattern similar to that of a perfect piston source. Following this procedure, the value of $G_T(\alpha_o)_{avg}$ can be calculated for the XONICS sounder. Assuming the XONICS acoustic transmitting array to approximate that of a perfect piston source (WD Neff of the Wave Propagation Laboratory), a good approximation of the gain can be predicted from diffraction theory (ref 25) as:

$$G_T(\alpha_o)_{avg} = \frac{G_T(o)\lambda^2 L_T(\alpha_o)}{\pi\alpha_o^2 A_T} = G_T(o)D_T(\alpha_o)_{avg} \,. \tag{A3}$$

where $G_T(o)$ is the transmitter on axis gain, λ is the acoustic wavelength, A_T is the transmitting antenna aperture area, and $L_T(\alpha_o)$ is a Bessel function of the form:

$$L_T(\alpha_o) = 1 - J_o^2\left(\frac{2\pi a\alpha_o}{\lambda}\right) - J_1^2\left(\frac{2\pi a\alpha_o}{\lambda}\right), \tag{A4}$$

where a is the radius of the transmitting antenna aperture.

The power backscattered from an effective illuminated volume, defined by a right circular cylinder of height $c\tau/2$, can be obtained by combining equations A3 and A2 and assuming that $D_T(\alpha_o)_{avg} = D_r(\alpha_o)_{avg}$ (monostatic case where the same antenna is used for both transmitting and receiving). This definition is:

$$P_r = \frac{P_T G C \tau A_r \sigma(\theta) L}{2R^2} \,, \tag{A5}$$

where G is the gain-compensation factor for the backscatter case and is given by:

$$G = \frac{G_T(o)\lambda^4 L^2(\alpha_o)}{4\pi^2\alpha_o^2 A_T^2} \,. \tag{A6}$$

Equation A5 is the standard backscatter acoustic-radar equation for monostatic acoustic sounding. However, for bistatic operation, equation A5 does not apply since $D_T(\alpha_o)_{avg} \neq D_r(\alpha_o)_{avg}$ (separate transmitting and receiving antennas) and the effective illuminated volume is no longer a right circular cylinder of height $C\tau/2$. The scattering volume for bistatic operation is now defined as that volume formed by the intersection of the conical transmitter beam and ellipsoidal surfaces with foci at the points of emission (transmitter) and reception (receiver) forming the upper and lower bounds of the illuminated volume. The surfaces are ellipsoidal such that energy scattered at different times by different points on any one surface will arrive at the receiver (located at the foci point) at the same time. Figure A1 shows a vertical plane of the scattering volume defined by the ellipsoidal surfaces.

---

25. Born, M and Wolf, E, Principles of Optics, p 295-395, MacMillan, New York, 1964

The effective height of the pulse-illuminated volume for bistatic operation can be calculated from the geometrical configuration of the scattering volume. At time, t, acoustic energy, which is scattered from all points along the lower ellipsoidal surface as well as by all points lying below the surface, arrives at the receiver. At time, $t+\Delta t$, the received scattered signal will be from the upper ellipsoidal surface located at some distance, $C\Delta t$, above the lower surface. The height, h, is defined as that height where the power scattered at a scattering angle, θ, by particles along the upper ellipsoidal surface from the front of the outgoing pulse of length, $C\tau$, will arrive at the receiver at the same time as the power scattered by particles along the lower ellipsoidal surface from the rear of the outgoing pulse. The height, h, is a function of scattering angle, θ, and pulse length, τ, and is given by:

$$h = \frac{C\tau}{(1-\cos\theta)} \quad . \tag{A7}$$

Equation A7 is in agreement with the results of Kallistratova (ref 26).

Calculation of the pulse-illuminated volume, V, taking into account the ellipsoidal surfaces, is complex. Therefore, an approximate calculation of V was made assuming that: the ellipsoidal surfaces forming the upper and lower bounds of the illuminated volume may be replaced by plane surfaces and the resulting plane surfaces are parallel to each other. The illuminated volume is then assumed to be approximated by a cylinder whose cross section is a parallelogram of height, h (eq A7), and radius, $R_1\alpha_o$ (fig A1). Since the bounding planes of the cylinder are assumed to be parallel, the volume is that of a right circular cone and is given by (utilizing equation A7):

$$V = \pi(R_1\alpha_o)^2\, h = \frac{\pi R_1^2 \alpha_o^2 C\tau}{(1-\cos\theta)} \quad . \tag{A8}$$

Combining equations A2, A3, and A8, one obtains the scattered power:

$$P_r = \frac{P_T C\tau A_r \sigma(\theta) L}{R_2^2(1-\cos\theta)} \left[\frac{G_T(o)\lambda^2 L_T(\alpha_o) D_r(\alpha_o)_{avg}}{4\pi A_T}\right], \tag{A9}$$

where the quantity in brackets is the beam-shaping compensation factor, G′, for the bistatic sounder system. The quantity, G′, contains separate parameters describing both the transmitter and bistatic receiver antennas. Rewriting equation A9, we get:

$$P_r = \frac{P_T G' C\tau A_r \sigma(\theta) L}{R_2^2(1-\cos\theta)} \quad , \tag{A10}$$

---

26. Kallistratova, MA, "Experimental Investigation of Sound Wave Scattering in the Atmosphere," Trudy Instituta, Fiziki Atmosfery, Atmosfernaya Turbulentnost, No 4, p 203-256 (translated by Foreign Technology Division, Translation FTD-TT-63-441/1 + 2 + 4), 25 June 1963

where

$$G' = \frac{G_T(o)\lambda^2 L_T(\alpha_o) D_r(\alpha_o)_{avg}}{4\pi A_T} \quad . \tag{A11}$$

Evaluation of the beam-shaping compensation factor, G', (eq A11), for the bistatic XONICS sounder requires that $D_r(\alpha_o)_{avg}$ be evaluated for the fan-beam bistatic receiver antennas. These antennas have beam widths of 65^o in the horizontal and 36^o in the vertical and cannot be treated as perfect piston sources with circular apertures. The evaluation of $D_r(\alpha_o)_{avg}$ is, therefore, very complex and does not follow the development by *Hall and Wescott (ref 24)*. Since this complex development is not within the scope of this study, the value of the compensation factor for the bistatic acoustic-sounder case will be assumed to closely approximate that given by Hall and Wescott (ref 24) for the monostatic case, ie, $G' \approx 0.24$.

Including the efficiency of the conversion of the transmitted electrical to acoustical energy (E_T), the effective receiver antenna aperture factor (E_r), and the molecular attenuation factor ($L = e^{-k(R_1 + R_2)}$), equation A10 for the available acoustic power from the receiving antenna is given by:

$$P_r = \left[P_T \cdot E_T \cdot G'\right]\left[\frac{C\tau}{(1-\cos\theta)} \cdot \frac{A_r}{R_2^2} \cdot E_r\right]\left[e^{-k(R_1 + R_2)}\right]\sigma(\theta) \quad . \tag{A12}$$

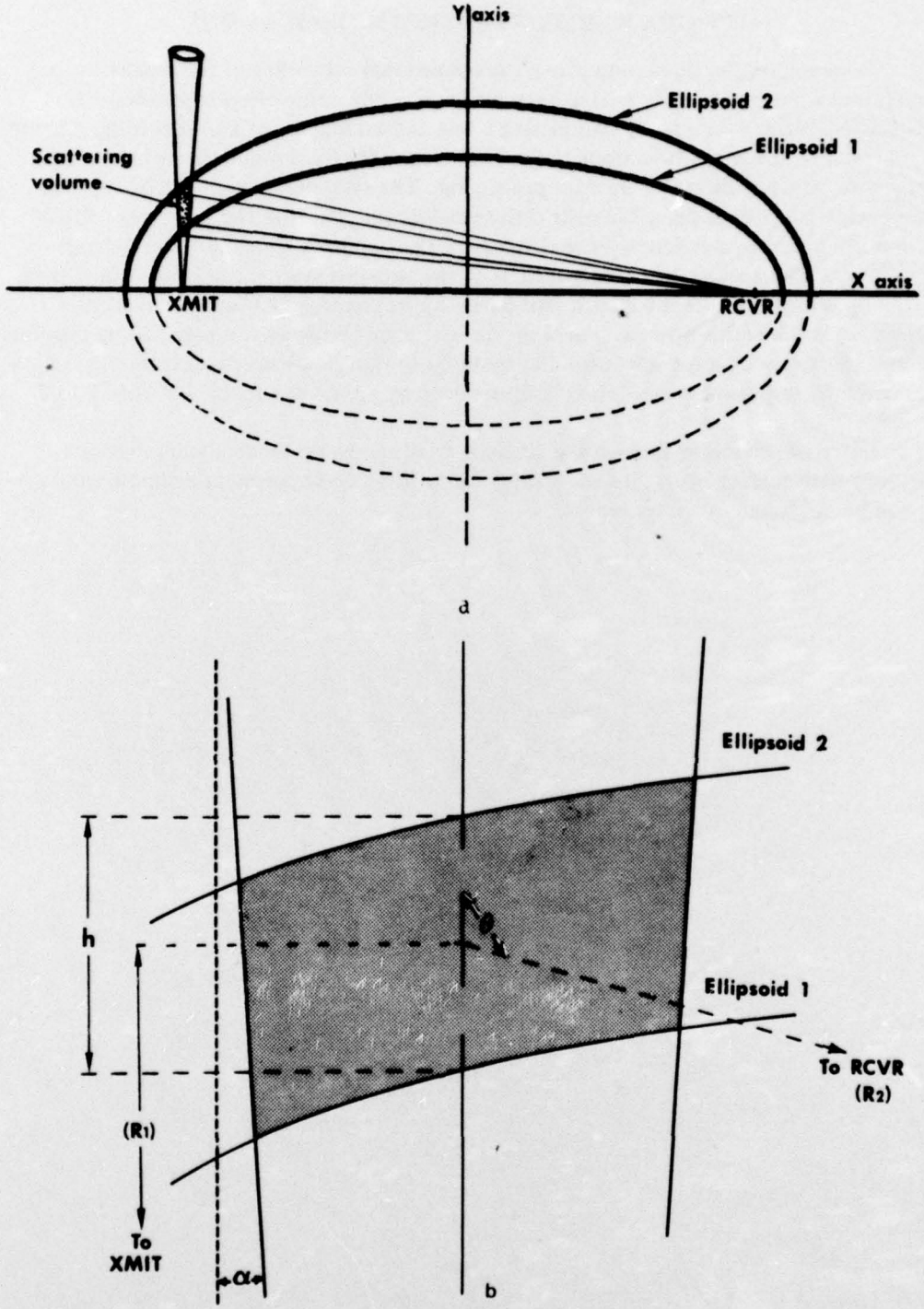

Figure A1. Geometrical configuration of scattering volume for bistatic acoustic echo sounding: (a) Vertical plane view showing the scattering volume defined by the conical transmitter beam and the ellipsoidal surfaces (z axis out of page); (b) Expanded view of scattering volume shown in (a).

APPENDIX B: RECENT SYSTEM MODIFICATIONS

System modifications to improve the operational capability of the acoustic echo-sounder and wind-sensor system have been made since the completion of this report. XONICS INC, after successfully completing a test and evaluation of a similar doppler wind system (ref 27), made modifications to the NELC sounder to improve the signal-to-noise ratio and to improve the software data processing. The system now consists of two fan-beam receiving antennas placed in near orthogonal directions from the transmitter (two-axis system) and provides time-averaged values of the two-orthogonal horizontal wind components. The geometrical configuration of the two-axis system can be imagined from figure 3 by relocating antenna 2 such that θ_{12} is approximately 90° and eliminating antenna 3. Antenna 2 is now in an area of lower ambient noise as compared to its previous location. Software changes were also incorporated to reduce doppler spectrum contamination caused by impulsive noise. The minimum averaging time was increased from 1 to 2 minutes.

Initial observations showed the acoustic winds to be reasonable and in general agreement with surface observations. Evaluation of the two-component acoustic wind system will be published in a later report.

27. NOAA Technical Memorandum ERL-WDL-16, Performance Test Results for a XONICS Acoustic Doppler Sounder, by Duane A Haugen, May 1976

APPENDIX C: REFERENCES

1. Lane, JA and RW Meadows, "Simultaneous Radar and Refractometer Soundings of the Troposphere," Nature, v 197, p 35-36, 1963

2. Atlas, D, KR Hardy, and KM Glover, "Multi-wavelength Backscatter from the Clear Atmosphere," Proceedings of the International Colloquium on Atmospheric Turbulence and Radio Propagation (Eds Yaglom and Tatavski, Moscow), p 249-260, 1965

3. Ottersten, H and F Eklund, "Radar Angle Activity and its Correlation with Meteorological Parameters," Proceedings of the International Colloquium on Atmospheric Turbulence and Radio Propagation (Eds Yaglom and Tatavski, Moscow), p 269-277, 1965

4. Fehlhaber, L and J Grosskopf, "Untersuchung der Struktur der Troposphäre mit einem Vertikalradar," Nachrichtentechnische Zeitschrift, v 17, p 503-507, 1964

5. Richter, JH, "High Resolution Tropospheric Radar Sounding," Radio Science, v 4, no 12, p 1261-1268, December 1969

6. McAllister, LG, "Acoustic Sounding at the Lower Troposphere," Journal of Atmospheric Terrestrial Physics, v 30, p 1439-1440, 1968

7. Little, CG, "Acoustic Methods for the Remote Probing of the Lower Atmosphere," Proceedings of the IEEE, v 57, no 6, p 571-578, April 1969

8. Lighthill, MJ, "On the Energy Scattered from the Interaction of Turbulence with Sound or Shock Waves," Proceedings of the Philosophical Society, v 49, p 531-555, 1953

9. Kraichnan, RH, "The Scattering of Sound in a Turbulent Medium," Journal of the Acoustical Society of America, v 25, p 1096-1104, 1953

10. NAS-NRC Publication 515, Proceedings of the Symposium on Naval Hydrodynamics, "Wave Scattering due to Turbulence," by GK Bachelor, p 409-430, 1957

11. Monin, AS, "Characteristics of the Scattering of Sound in a Turbulent Atmosphere," Akust Zh 7, p 457-461, 1961 (English translation from Soviet Physical Acoustics, v 7, p 370-372)

12. Kologorov, AH, "The Local Structure of Turbulence in an Incompressible Viscous Fluid for Very Large Reynolds Number," Dokl Akad, Nauk SSSR 30, p 301, 1941

13. XONICS, Inc, Technical Manual and Software Description for the NELC Wind Sensor System, TR-50, March 1974

14. Naval Electronics Laboratory Center Technical Report 1849, Simultaneous FM-CW Radar and Lidar Probing of the Atmosphere, by VR Noonkester, DR Jensen, and JH Richter, 1 November 1972

15. Naval Electronics Laboratory Center Technical Report 1862, Meteorological Processes and FM-CW Radar Soundings in the Boundary Layer, by VR Noonkester, DR Jensen, JH Richter, 5 February 1973

16. Hall, FF, Jr. "Temperature and Wind Structure Studies by Acoustic Echo-Sounding," Remote Sensing of the Troposphere (VE Derr, editor), National Oceanic and Atmospheric Administration, p 18-1 to 18-25, August 1972

17. Gossard, EE, JH Richter, and D Atlas, "Internal Waves in the Atmosphere from High-Resolution Radar Measurements," Journal of Geophysical Research, v 75, no 18, p 3523–3536, June 1970

18. Beran, DW and FF Hall, Jr, "Remote Sensing Applications in Air-Pollution Meteorology," Second Joint Conference on Sensing of Environmental Pollutants (reprint), p 231–246, Instrument Society of America, December 1973

19. Hooke, WH, JM Young, and DW Bean, "Atmospheric Waves Observed in the Planetary Boundary Layer Using an Acoustic Sounder and a Microbarography Array," Boundary Layer Meteorology, v 2, p 371–380, 1972

20. Richter, JH and DR Jensen, "Simultaneous Acoustic Sounder and FM-CW Radar Observations," 16th Radar Meteorology Conference (preprint), p 282–289, American Meteorological Society, April 1975

21. Gossard, EE, JH Richter, and DR Jensen, "Effect of Wind Shear on Atmosphere Wave Instabilities Revealed by FM-CW Radar Observations," Boundary Layer Meteorology, v 4, p 113–131, 1973

22. Willmarth, BC, EH Brown, JT Priestly, and DW Beran, "Beam Pattern Measurements for Large Acoustic Antennas," 16th Radar Meteorology Conference (preprints), p 278–281, American Meteorological Society, April 1975

23. Richter, JH and DR Jensen, "New Developments in the Detection of Atmospheric Structures," Proceedings of the NATO Advanced Study Institute on Atmospheric Effects on Target Identification and Classification, Goslar, Germany (in press)

24. Hall, FF and JW Wescott, "Acoustic Antennas for Atmospheric Echosounding," Journal of the Acoustic Society of America, v 56, no 5, p 1376–1382, November 1974

25. Born, M and Wolf, E, Principles of Optics, p 395–398, MacMillan, New York, 1964

26. Kallistratova, MA, "Experimental Investigation of Sound Wave Scattering in the Atmosphere," Trudy Instituta, Fiziki Atmosfery, Atmosfernaya Turbulentnost, No 4, p 203–256 (translated by Foreign Technology Division, Translation FTD-TT-63-441/1+2+4), 25 June 1963

27. NOAA Technical Memorandum ERL-WDL-16, Performance Test Results for a XONICS Acoustic Doppler Sounder, by Duane A Haugen, May 1976